Transmission of THz radiation through InSb gratings of subwavelength apertures

Jaime Gómez Rivas, Christof Janke, Peter Haring Bolivar and Heinrich Kurz

Institut für Halbleitertechnik, RWTH Aachen, Sommerfeldstr. 24, D-52056 Aachen, Germany.

Jaime.Gomez@THz-photonics.com

Abstract: We demonstrate the extraordinary transmission of terahertz THz radiation through gratings of subwavelength apertures structured in indium antimonide InSb. This transmission can be attributed to the tunneling of surface plasmons polaritons which are excited in semiconductors at THz frequencies. By thermally controlling the permittivity of the grating the transmittance increases by more than one order of magnitude. This increase might be associated to the larger the skin depth in InSb at low temperatures, which gives rise to a larger effective size of the apertures.

References and links

1. T.W. Ebbesen, H.J. Lezec, H.F. Ghaemi, T. Thio, and P.A. Wolff, "Extraordinary optical transmission through sub-wavelength hole arrays," Nature **391**, 667-669 (1998).
2. H.F. Ghaemi, T. Thio, D.E. Grupp, T.W. Ebbesen, and H.J. Lezec, "Surface plasmons enhance optical transmission through subwavelength holes," Phys. Rev. B **58**, 6779-6782 (1998).
3. T. Thio, H.F. Ghaemi, H.J. Lezec, P.A. Wolff, and T.W. Ebbesen, "Surface-plasmon-enhanced transmission through hole arrays in Cr films," J. Opt. Soc. Am B **16**, 1743-1748 (1999).
4. W.L. Barnes, A. Dereux, and T.W. Ebbesen, "Surface plasmon subwavelength optics," Nature **424**, 824 (2003).
5. L. Martín-Moreno, F.J. García-Vidal, H.J. Lezec, K.M. Pellerin, T. Thio, J.B. Pendry, and T.W. Ebbesen, "Theory of extraordinary optical transmission through subwavelength hole arrays," Phys. Rev. Lett. **86**, 1114 (2001).
6. S. Enoch, E. Popov, M. Neviere, and R. Reinisch, "Enhanced light transmission by hole arrays," J. Opt. A: pure Appl. Opt. **4**, S83 (2002).
7. W.-C. Liu, D.P. Tsai, "Optical tunneling effect of surface plasmon polaritons and localized plasmon resonance," Phys. Rev. B **65**, 155423 (2002).
8. S.A. Darmanyan and A.V. Zayats, "Light tunneling via resonant surface plasmon polariton states and the enhanced transmission of periodically nanostructured metal films: an analytical study," Phys. Rev. B **67**, 035424 (2003).
9. M.M.J. Treacy, "Dynamical diffraction explanation of the anomalous transmission of light through metallic gratings," Phys. Rev. B **66**, 195105 (2002).
10. H.J. Lezec and T. Thio, "Diffracted evanescent wave model for enhanced and suppressed optical transmission through subwavelength hole arrays," Opt. Express **12**, 3629 (2004), http://www.opticsexpress.org/abstract.cfm?URI=OPEX-12-16-3629.
11. L. Martín-Moreno, F.J. García-Vidal, H.J. Lezec, A. Derigon, and T.W. Ebbesen, "Theory of highly directional emission from a single subwavelength aperture surrounded by surface corrugations," Phys. Rev. Lett. **90**, 167401 (2003).
12. J.B. Pendry, L. Martín-Moreno, and F.J. García-Vidal, "Mimicking surface plasmons with structured surfaces," Science **305**, 847 (2004).
13. M. Lockyear, A.P. Hibbins, J.R. Sambles, and C.R. Lawrence, "Surface-topography induced enhanced transmission and directivity of microwave radiation through subwavelength circular metal aperture," Appl. Phys. Lett. **84**, 2040 (2004).

14. D. Qu, D. Grischkowsky, and W. Zhang, "Terahertz transmission properties of thin subwavelength metallic hole arrays," Opt. Lett. **29**, 896 (2004).

15. H. Cao and A. Nahata, "Resonantly enhanced transmission of terahertz radiation through a periodic array of subwavelength apertures," Opt. Express **12**, 1004 (2004), http://www.opticsexpress.org/abstract.cfm?URI=OPEX-12-6-1004.

16. F. Miyamaru and M. Hangyo, "Finite size effect of transmission property for metal hole arrays in subterahertz region," Appl. Phys. Lett. **84**, 2742 (2004).

17. S.S. Akarca-Biyikli, I. Bulu, and E. Ozbay, "Enhanced transmission of microwave radiation in one-dimensional metallic gratings with subwavelength aperture," Appl. Phys. Lett. **85**, 1098 (2004).

18. J. Gómez Rivas, C. Schotsch, P. Haring Bolivar, and H. Kurz, "Enhanced transmission of THz radiation through sub-wavelength holes," Phys. Rev. B **68**, 201306 (2003).

19. C. Janke, J. Gómez Rivas, C. Schotsch, L. Beckmann, P. Haring Bolivar, and H. Kurz, "Optimization of the enhanced THz transmission through arrays of sub-wavelength apertures," Phys. Rev. B **69**, 205314 (2004).

20. J. Gómez Rivas, P. Haring Bolivar, and H. Kurz, "Thermal switching of the enhanced transmission of THz radiation through sub-wavelength apertures," Opt. Lett. **29**, 1680 (2004).

21. The transmission efficiency in Refs. [18, 19, 20] was defined as the transmitted amplitude normalized by the fraction of the surface occupied by the apertures, in contrast to the definition adopted here which refers to the transmitted power.

22. D.E. Grupp, H.J. Lezec, T.W. Ebbesen, K.M. Pellerin, and T. Thio, "Crucial role of metal surface in enhanced transmission through subwavelength apertures," Appl. Phys. Lett. **77**, 1569-1571 (2000).

23. M. van Exter and D. Grischkowsky, "Optical and electronic properties of doped silicon from 0.1 to 2 THz," Appl. Phys. Lett. **56**, 1694-1696 (1990).

24. O. Madelung, "Physics of III-V compounds," Chapter 4 (John Wiley & Sons, Inc., New York 1964).

25. S.C. Howells and L.A. Schlie, "Transient terahertz reflection spectroscopy of undoped InSb from 0.1 to 1.1 THz," Appl. Phys. Lett. **69**, 550 (1996).

26. CrysTec GmbH, www.crystec.de.

27. U. Schröter and D. Heitmann, "Surface-plasmon-enhanced transmission through metallic gratings," Phys. Rev. B **58**, 15419 (1998).

28. J.A. Porto, F.J. García-Vidal, and J.B. Pendry, "Transmission resonances on metallic gratings with very narrow slits," Phys. Rev. Lett. **83**, 2845 (1999).

29. S. Astilean, Ph. Lalanne, and M. Palamaru, "Light transmission through metallic channels much smaller than the wavelength," Opt. Comm. **175**, 265 (2000).

30. H.E. Went, A.P. Hibbins, J.R. Sambles, C.R. Lawrence, and A.P. Crick, "Selective transmission through very deep zero-order metallic gratings at microwave frequencies," Appl. Phys. Lett. **77**, 2789 (2000).

31. A.P. Hibbins, J.R. Sambles, C.R. Lawrence, and D.M. Robinson, "Remarkable transmission of microwave through a wall of long metallic bricks," Appl. Phys. Lett. **79**, 2844 (2001).

32. Q. Cao and P. Lalanne, "Negative Role of Surface Plasmons in the Transmission of Metallic Gratings with Very Narrow Slits," Phys. Rev. Lett. **88**, 057403 (2002).

33. S. Collin, F. Pardo, R. Teissier, and J.-L. Pelouard, "Horizontal and vertical surface resonances in transmission metallic gratings," J. Opt. A **4**, S154 (2002).

34. P. Lalanne, C. Sauvan, J.P. Hugonin, J.C. Rodier, and P. Chavel, "Perturbative approach for surface plasmon effects on flat interfaces periodically corrugated by subwavelength apertures," Phys. Rev. B **68**, 125404 (2003).

35. J.L. Adams, L.C. Botten, and R.C. McPhedran, "The crossed lamellar transmission grating," J. Optics **9**, 91 (1978).

36. D.R. Grischkowsky, S. Keiding, M. van Exter, and C. Fattinger, "Far-infrared time-domain spectroscopy with terahertz beams of dielectrics and semiconductors," J. Opt. Soc. Am. B **7**, 2006 (1990).

37. R.W. Wood, "Anomalous diffraction gratings," Phys. Rev. **48**, 928 (1935).

38. K.J.K. Koerkamp, S. Enoch, F.B. Segerink, N.F. van Hulst, and L. Kuipers, "Strong influence of hole shape on extraordinary transmission through periodic arrays of subwavelength holes," Phys. Rev. Lett. **92**, 183901 (2004).

39. A. Degiron, H.J. Lezec, W.L. Barnes, and T.W. Ebbesen, "Effects of hole depth on enhanced light transmission through subwavelength hole arrays," Appl. Phys. Lett. **81**, 4327 (2002).

40. H. Raether, "Surface plasmons on smooth and rough surfaces and on gratings," Springer Tracts in Modern Physics, vol. 111 (Springer-Verlag, Berlin 1988).

41. L. Martín-Moreno and F.J. García-Vidal, "Optical transmission through circular hole arrays in optically thick metal films," Opt. Express **12**, 3619 (2004), http://www.opticsexpress.org/abstract.cfm?URI=OPEX-12-16-3619.

42. J.D. Jackson, "Classical electrodynamics," thrid edition, Chapter 8 (John Wiley & Sons, Inc., New York 1999).

1. Introduction

The recent discovery of the extraordinary transmission of light through gratings of nanoholes [1, 2] in metal films has opened a new field of intensive research. Defining the transmission effi-

ciency as the transmitted intensity normalized to the fraction of the grating's surface occupied by the holes, transmission efficiencies even higher than 100% have been reported [3], i.e., more light than that incident on the holes is transmitted. Beaming light through structures smaller than the wavelength of the radiation has potential applications in fields such as optical data storage, near field microscopy, and optical displays [4]. This anomalous transmission has been explained by the resonant tunneling of surface waves such as surface plasmon polaritons SPPs [5, 6, 7, 8]: the incident radiation on one side of the film is coupled to SPPs via a periodic corrugation of its surface. Surface plasmons generate a large electromagnetic field close to the surface and enhance the transmission through the apertures. Although this view is widely accepted, explanations of this phenomenon based on diffraction theory have been proposed [9, 10].

Most of the work in this field has been done at optical and near infrared frequencies. The very large and mainly imaginary permittivity of metals at low frequencies, i.e., far-infrared, THz and microwaves, was believed to be a limitation for the scalability of the enhanced transmission over the electromagnetic spectrum. However, it has been predicted that the corrugation on the surface of the metal surface defines an effective permittivity and plays a dominant role in the enhancement [11, 12]. It is therefore possible to excite SPPs in metal films at much lower frequencies. A few works have demonstrated the enhanced transmission of low frequency electromagnetic radiation [13, 14, 15, 16, 17].

We recently demonstrated a complementary approach for the transmission of THz radiation through subwavelength apertures [18, 19, 20]. This approach consists in using doped semiconductors instead of metals for the excitation and tunneling of low frequency SPPs. Doped semiconductors have at these frequencies permittivities with values closer to those of metals at optical frequencies, which should favor the scalability of the enhanced transmission over the electromagnetic spectrum. In Refs. [18, 19, 20], the transmission through square gratings of apertures structured in doped silicon was investigated. Significant transmissions at wavelengths much larger than the cutoff wavelength were reported, and transmission efficiencies up to $\simeq$ 15% were obtained through apertures up to fourfold smaller than the wavelength [21]. Nonetheless, the transmission through these gratings is still low compared to the optical transmission through similar gratings structured in good metals and comparable to the optical transmission through gratings in lossy metals [22].

In this article we present transmission measurements of THz radiation through gratings of subwavelength apertures structured in undoped Indium antimonide. InSb has a dominantly real permittivity at THz frequencies like that of good metals in the optical range. By varying the temperature of the grating we change its dielectric properties, modifying the transmission through the apertures. The transmittance at the resonance frequency can be varied by more than an order of magnitude in the temperature range from 325 to 225 K. An explanation of this change might be the variation of the skin depth of InSb, which modifies the effective size of the apertures. Although the grating structure and dimensions are not optimized, we obtain a maximum transmission efficiency as high as 50% through apertures with a nominal size ninefold smaller than the wavelength of the radiation. The increase of the subwavelength transmission at low temperatures is in contrast with the previously reported decrease of the transmission through gratings of doped Si, and with the temperature independent transmission through metallic gratings [20].

The article is divided as follows: The dielectric properties of InSb at terahertz frequencies and their dependence with temperature are described in section 2.1. In section 2.2 we explain the procedure used to fabricate the gratings. The experimental technique employed to measure the transmission through the gratings, i.e., THz time-domain spectroscopy, is explained in section 3.1. In section 3.2 we present the transmission measurements at 325 K. The thermal switching and tuning of the transmission are discussed in section 4.

2. Samples

2.1. Material properties

Surface plasmon polaritons are electromagnetic waves which are coupled to the oscillation of free charges, and that propagate along the surface of conducting materials. A conductor is characterized by a complex permittivity ($\varepsilon = \varepsilon' + i\varepsilon''$) with a negative ε'. A large ε'' is characteristic of lossy metals. Optical experiments have shown that larger enhancements of the transmission are achieved in gratings with small ε'' compared to ε' [22]. The highest transmission efficiencies have been observed in gratings structured in silver, which has a permittivity of $\varepsilon \simeq -33 + 3i$ at 800 nm. However, at low frequencies metals have very large and dominantly imaginary permittivities. The permittivity of silver at 1 THz, i.e. 300 μm, is $\varepsilon = -2.4 \cdot 10^5 + 10^6 i$.

Alternative materials for the excitation of low frequency surface plasmons are semiconductors. Semiconductors have a permittivity at low frequencies close to that of metals at optical frequencies. This permittivity $\varepsilon(\omega)$ is well described by the Drude model [23]

$$\varepsilon(\omega) = \varepsilon_\infty \left(1 - \frac{\omega_p^2}{\omega^2 + \tau^{-2}} + i\frac{\omega_p^2 \tau^{-1}}{\omega(\omega^2 + \tau^{-2})} \right) \tag{1}$$

where ε_∞ is the high-frequency permittivity, τ is the average collision time of the charge carriers and $\omega_p = \sqrt{Ne^2/\varepsilon_\infty\varepsilon_0 m^*}$ is the plasma frequency. The semiconductor charge carrier concentration is given by N, while e is the fundamental charge, ε_0 the vacuum permittivity and m^* the charge carrier effective mass. The carrier mobility μ is related to τ by $\mu = \tau e/m^*$. InSb is a semiconductor with a very small energy gap of 0.17 eV and a very large electronic mobility $\simeq 7.7 \cdot 10^4 \text{cm}^2 \text{V}^{-1} \text{s}^{-1}$ [24]. At room temperature InSb has an intrinsic carrier concentration of $\simeq 10^{16} \text{cm}^{-3}$. The electron effective mass in InSb is 0.014 m_0, where m_0 is the electron mass and $\varepsilon_\infty = 15.7$.

In Fig. 1 are plotted the values of $|\varepsilon'|$ and ε'' calculated with Eq. (1) and assuming that holes do not contribute to the metallic character of InSb. This assumption is justified by the much lower mobility of holes in comparison to the electronic mobility, which makes the contribution of holes to the complex permittivity negligible [25]. The absolute value of the permittivity of InSb is much lower than that of metals at THz frequencies. Moreover $|\varepsilon'|$ is larger than ε'' at these frequencies.
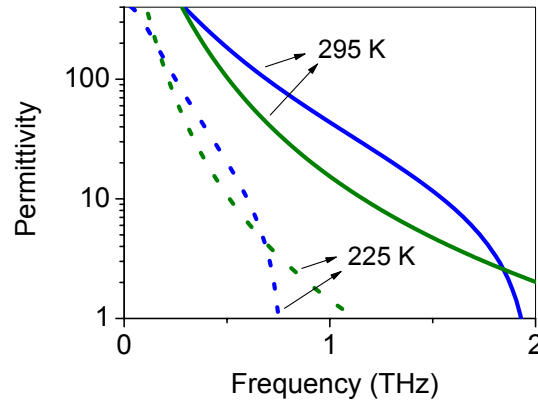

Fig. 1. Absolute value of the real part (blue lines) and the imaginary part (green lines) of the complex permittivity of InSb versus the frequency calculated with the Drude model. The solid curves correspond to room temperature, while the dashed curves are the permittivity at 225 K.
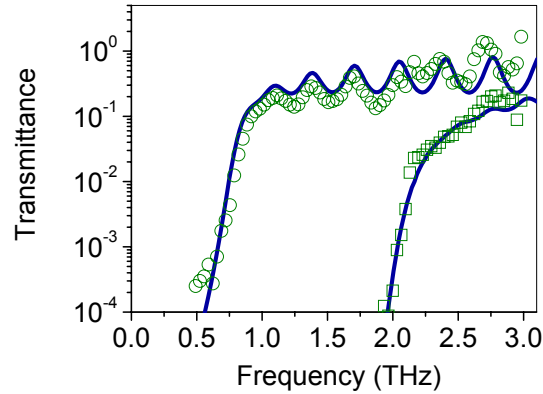
Fig. 2. Transmittance measurements through a slab of bulk InSb with a thickness of 100 μm. The squares are measurements at room temperature, while the circles correspond to measurements at 225 K. The solid curves are fits to the measurements using the values of the permittivity calculated with the Drude model.

A great advantage of semiconductors over metals is that their permittivity can be easily modified, which affects the SPPs characteristics and the subwavelength transmission [20]. According to Eq. (1), the permittivity depends on the charge carrier density N and mobility μ. These quantities can be varied by changing the temperature: as the temperature is lowered the number of thermally excited carriers is reduced and their mobility increases. In InSb at 225 K we have $N \simeq 0.2 \cdot 10^{16}$ cm^{-3} and $\mu \simeq 13.4 \cdot 10^4$ cm^{2}V^{-1}s^{-1}. The permittivity of InSb at 225 K is plotted in Fig. 1 with dashed curves. As can be seen, a significant change in the permittivity can be achieved by varying the temperature only 70 K.

Figure 2 displays transmission measurements through a slab of InSb with a thickness of 100 μm. These measurements were done with a THz time-domain spectrometer as it is explained in detail in the next section. At this point we only want to show the strong variation of the THz transmission through InSb with temperature due to the modification of its permittivity. The squares in Fig. 2 correspond to the measurements at room temperature, whereas the circles are the measurements at 225 K. As the temperature is reduced the plasma frequency shifts to lower values due to the reduction of free carriers. At frequencies larger than $\omega_{\rm p}/2\pi$ the semiconductor behaves as a dielectric and the transmission increases. Multiple reflections at the interfaces of the InSb slab give rise to the oscillation on the high frequency transmittance. The very low transmittance at frequencies lower than $\omega_{\rm p}/2\pi$ is due to the metallic behavior of InSb.

The solid curves in Fig. 2 are fits to the transmission measurements taking the electronic mobility given in literature [24] and adjusting the carrier density. The carrier densities obtained from the fits, i.e., $1.1 \cdot 10^{16}$ cm^{-3} at room temperature and $0.2 \cdot 10^{16}$ cm^{-3} at 225 K, are in good agreement with the values given in literature. The values of the complex permittivity at a frequency of 0.6 THz obtained experimentally at different temperatures are displayed in Table 1.

2.2. *Grating fabrication*

To structure the grating of subwavelength apertures a commercially available undoped InSb wafer [26] with a thickness of 500 μm was lapped and polished to a thickness of 130 ± 5 μm. Parallel cuts with a depth of 90 ± 5 μm, a width of 65 ± 5 μm and spaced by 300 ± 10 μm were done on one side of the wafer with a wafer dicing saw (Disco DAD 321). Perpendicular cuts to these, with the same depth, width and spacing, were done on the opposite side of the wafer. This

Table 1. Real ε' and imaginary ε'' permittivities of InSb at 0.6 THz for different temperatures T. Also are listed the propagation length of SPPs δ_{SPP} on flat interfaces between air and a material with permittivity $\varepsilon = \varepsilon' + i\varepsilon''$, the skin depth of the material δ_{InSb}, and the SPPs decay length into air δ_{air}.

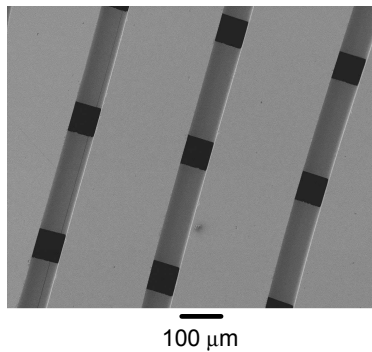| T(K)	ε'	ε''	δ_{SPP} (cm)	δ_{InSb} (μm)	δ_{air} (mm)
325	-200	110	5.7	5.6	1.1
295	-133	64	4.3	6.9	0.91
270	-67	33	2.1	9.6	0.65
255	-49	22	1.7	11.3	0.55
240	-25	12	0.8	15.6	0.39
225	-10	6	0.2	23.9	0.24

100 μm

Fig. 3. Scanning electron microscope image of a grating of subwavelength apertures structured in InSb. The thickness of the the grating is 130 μm, the lattice constant 300 μm, and the lateral size of the apertures 65 μm.

process creates a square grating of apertures with a lattice constant of 300 ± 10 μm. The square side of the apertures is 65 ± 5 μm. In Fig. 3 a top view of the grating taken with a scanning electron microscope is displayed. The dark squares in this photograph are the apertures.

The transmission through metallic lamellar gratings or gratings with narrow slits has been intensively studied in recent years [27, 28, 29, 30, 31, 32, 33, 34]. The enhanced transmission through these structures is explained by the excitation of coupled SPPs on both surfaces of the grating and the resonances in the cavities [28]. Our samples are more complex and less thoroughly investigated than lamellar gratings, as they can been viewed as crossed lamellar transmission gratings with a negative array separation distance [35].

3. THz time domain spectroscopy

3.1. Experimental setup

For the experiments we use a THz time-domain spectrometer [36], in which a train of femtosecond pulses from a Ti:sapphire laser is split to generate and detect single-cycle terahertz pulses. The Ti:sapphire pulses produce THz radiation on an InGaAs surface field emitter. This radiation is collected by a parabolic mirror and focused onto the sample. The beam diameter on the sample is $\simeq 1.5$ mm and the beam divergence 150 mrad. The transmitted radiation through the grating is focused onto a photoconductive antenna, which is gated with the pulses of the
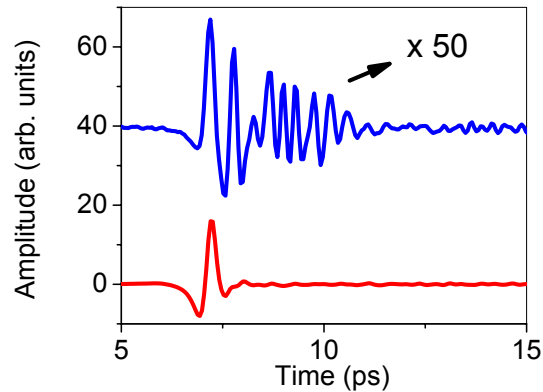
Fig. 4. Time-domain terahertz amplitude. The red curve corresponds to the setup response, while the blue curve is the transmission through a square grating of apertures structured in InSb. For clarity a vertical offset is introduced.

Ti:sapphire laser. By varying the path length difference between the generation and detection branches of the setup, the THz field amplitude can be detected as a function of time with sub-picosecond time resolution.

Figure 4 displays typical transients measured with our setup. The two measurements of Fig. 4 are vertically offset for clarity. The red curve is a reference measurement, which corresponds to the response of the setup. The blue curve is the transmitted amplitude through the InSb grating at room temperature. The grating markedly modifies the incident pulse: the transmitted amplitude is reduced and significant dispersion is introduced.

It is important to mention that THz time domain spectroscopy measures the amplitude and the phase of the THz pulse. Although the phase carries important information about the dynamic properties of the transmission, in this article we discuss only on the transmitted amplitude.

3.2. *Spectral transmission*

To further analyze the time domain measurements, we calculate the power spectrum by Fourier transforming the transients. The inset of Fig. 5 displays the power spectrum of the reference pulse. Defining the transmittance as the power spectrum of the transmitted pulse through the grating normalized by the power spectrum of the reference, the transmittance at 325 K is plotted in Fig. 5. The transmittance exhibits several local minima and a remarkable peak at a frequency of 0.6 THz. This frequency corresponds to a wavelength in vacuum of 500 μm, i.e., eight-fold larger than the lateral size of the apertures. The pronounced transmission at a wavelength much larger than the size of the apertures is similar to the extraordinary optical transmission through gratings of nanoholes [1], which was interpreted in terms of the grating assisted coupling of the incoming radiation to surface plasmon polaritons and the subsequent coupling back into radiation on the opposite side of the sample.

The minima in the transmittance at 1, 1.9, 2.3, 2.8 and 3 THz are in good agreement with the spectral positions of the Rayleigh-Wood's anomalies of a square grating with a lattice constant of 300 ± 10 μm. The Wood's anomalies are minima in the transmission spectrum of a grating due to the excitation of diffraction modes parallel to the sample surface [37]. For a square grating Wood's anomalies occur at wavelengths given by $\lambda = a_0/\sqrt{l^2 + m^2}$, where a_0 is the lattice constant of the grating, and l and m are integers. The spectral positions of the Wood's anomalies are indicated in Fig. 5 with dashed lines. Note that the Wood's anomaly expected at 1.4 THz is not apparent in the measurement, which might be due to the partial overlap
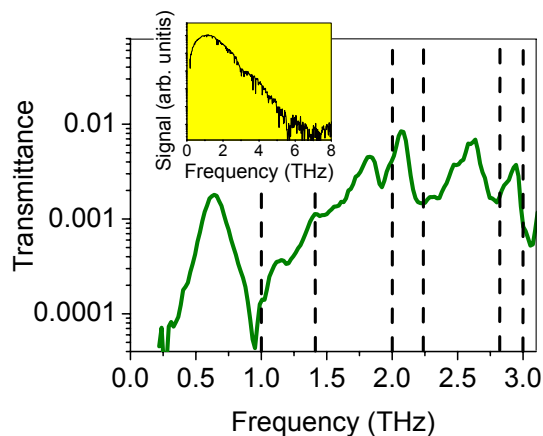
Fig. 5. Transmittance through a grating of InSb at a temperature of 325 K. The dashed lines indicate the frequencies of the Wood's anomalies for a square grating with a lattice constant of 300 μm. The inset represents the power spectrum of the reference pulse.

with high order SPPs resonances. The local maxima apparent above 1.5 THz between Wood's anomalies are mainly originated by the minimum transmission at these anomalies. Although there are two local maxima at 1.15 THz and 1.42 THz, which might be caused by high order resonances [2, 3, 18], these are not as pronounced as the maximum at 0.6 THz. Therefore, the discussion on the thermal tuning and switching presented in section 4.2 focuses in lowest frequency resonance.

It is important to mention that, in spite of the pronounced transmission at wavelengths much larger than the apertures, the structure and dimensions of the InSb grating have not been optimized. With the fabrication method that we employ (see section 2), we are only able to structure square gratings. A larger transmission through hexagonal arrays of holes has been demonstrated [3]. Also larger transmission has been reported in arrays of rectangular holes [38]. The transmission depends strongly with the thickness of the grating [19, 39]. In our gratings the minimum thickness is limited to about 100 μm by the fragility of the InSb wafers. Therefore, it is reasonable to expect a much larger THz transmissions than those presented here if the structure and dimensions of the grating are optimized. However, for this optimization, alternative fabrication methods are required.

4. Thermal switching and tuning

4.1. *Surface plasmon characteristic lengths*

As it was discussed in section 2, the permittivity of semiconductors can be easily varied by changing the temperature. This change will affect the SPPs characteristics and thus the sub-wavelength transmission. In this section we introduce briefly the SPP characteristic lengths for a flat interface between a conductor and air, and their dependence with the permittivity. This dependency will be used in the next section to explain qualitatively the increase of the resonant transmission through the InSb gratting at low temperatures.

For conductors with $|\varepsilon'| > \varepsilon''$, the propagation length of SPPs on a flat interface between the conductor and air can be approximated to [40]

$$\delta_{\text{SPP}} \simeq 2\frac{c_0}{\omega}\left(\frac{\varepsilon'+1}{\varepsilon'}\right)^{\frac{3}{2}}\frac{\varepsilon'^2}{\varepsilon''}\,,\tag{2}$$

where ω is the angular frequency, c_0 the speed of light in vacuum, and $\varepsilon = \varepsilon' + i\varepsilon''$ the complex permittivity of the conductor. According to Eq. (2), the propagation length decreases as ε' becomes smaller. Also when ε'' increases, i.e., when the dissipation of SPPs increases, the propagation length decreases.

Surface plasmon polaritons decay evanescently away from the surface. The decay length into air is given by

$$\delta_{\text{air}} \simeq \frac{c_0}{\omega} \left(\varepsilon' + 1 \right)^{\frac{1}{2}} . \tag{3}$$

Shorter decay lengths are thus obtained when ε' is small.

The decay length into the conductor or the skin depth of the conductor is given by

$$\delta_{\text{InSb}} \simeq \frac{c_0}{\omega} \left(\frac{\varepsilon' + 1}{\varepsilon'^2} \right)^{\frac{1}{2}} . \tag{4}$$

The skin depth is thus larger for small values of ε'. The values of δ_{SPP}, δ_{air} and δ_{InSb} on an InSb-air interface at different temperatures are listed in Table 1. As the temperature is lowered, the absolute values of ε' and ε'' decrease (see also Fig. 1), which gives rise to a larger skin depth and to a smaller decay length into air. As a consequence to the larger skin depth, SPPs are more effectively dissipated, which gives rise to a shorter δ_{SPP}.

4.2. Temperature dependent subwavelength transmission

The transmittance through the InSb grating at different temperatures is plotted in Fig. 6(a). The measurements correspond to 325 K (black line), 295 K (orange line), 270 K (purple line), 255 K (green line), 240 K (blue line), 225 K (red line). The transmission through a bulk piece of InSb with a thickness approximately equal to the effective thickness of the grating, i.e., 100 μm, is displayed in Fig. 6(b). As discussed in section 2, for low temperatures the plasma frequency of InSb shifts to lower frequencies due to the reduction of charge carrier density. Since InSb becomes transparent at frequencies higher than the plasma frequency, we are going to focus the following discussion on the low frequency range of the measurements, where the grating is opaque and the transmission takes place through the apertures. We note however that at 225 K the high transmittance through the grating at the resonant frequency of 0.6 THz might be partially caused by transmission through the thinnest regions of the grating, i.e., the cuts.

The resonant transmission at 0.6 THz increases and shifts to lower frequencies as the temperature is lowered. These changes can be also observed in the inset of Fig. 6, where we have plotted the transmittance at different temperatures in a linear scale as a function of the wavelength. The peak around 500 μm in the inset corresponds to the aforementioned resonant transmission at 0.6 THz.

The dependence with temperature of the resonant frequency and of the maximum transmittance are plotted in Figs. 7(a) and (b) respectively. In a moderately small temperature range of 100 K the resonant frequency shifts by more than 100 GHz and the maximum transmittance is increased by more than one order of magnitude. At 225 K the power transmission efficiency reaches 50% for apertures which are ninefold smaller than the resonant wavelength.

A possible qualitative explanation for the frequency shift of the transmission is the following. The coupling between radiation normally incident on a square grating with SPPs occurs at the frequencies [40]

$$\nu = \frac{c_0 \sqrt{l^2 + m^2}}{a_0} \frac{1}{n_{\text{eff}}}, \tag{5}$$

where a_0 is the lattice constant of the grating, l and m are integers, and n_{eff} is the effective refractive index for the coupling. The transmission through subwavelength apertures is maximum
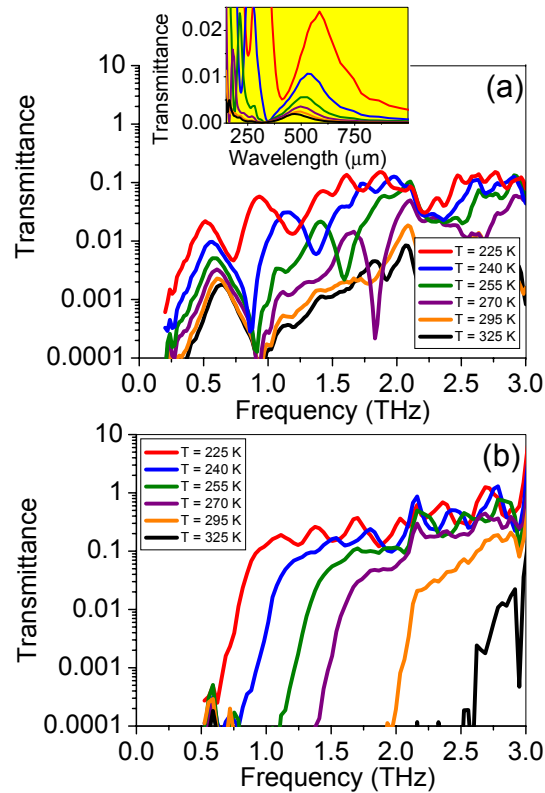
Fig. 6. (a) Transmittance through a grating of apertures with a lateral size of 65 μm structured in InSb. The transmittance is measured for different temperatures of the grating as indicated in the legenda. The inset represents the same measurements as a function of the wavelength. (b) Transmittance through a bulk piece of InSb with a thickness of 100 μm at different temperatures.

at approximately these frequencies, i.e., when the coupling between the SPPs and the radiation is optimum [1, 2]. The effective refractive index n_{eff} for an air-conductor interface is approximately given by $\sqrt{\varepsilon'/(1+\varepsilon')}$, i.e., approaches one when the absolute value of the permittivity of the material forming the grating is large. As the temperature of the InSb grating is lowered, its permittivity is reduced and n_{eff} increases, leading to an optimum coupling at lower frequencies. The temperature dependence of n_{eff} is represented in the inset of Fig. 7(a). We should stress that this is a qualitative description and Eq. (5) represents only a first approximation to the resonant frequency. This frequency appears in the InSb grating significantly shifted to lower values in contrast to similar measurements at optical frequencies [1, 2, 3]. Although a more rigorous theoretical description of the optical transmission through gratings of nanoholes [41] has confirmed that the resonance occurs at lower frequencies that those predicted by Eq. (5), we do not fully understand the cause of the large discrepancy between the optical and THz experiments.

At first sight the increase of the transmission at low temperatures is a surprising result because of the stronger SPPs dissipation at low temperatures (see Table 1). Therefore, another mechanism must compensate this dissipation. The finite skin depth δ_{InSb} in real metals has been identified to play an important role on the transmission of radiation through metallic lamellar gratings and 2D gratings [29, 41]. The simplest effect that a finite δ_{InSb} has is to increase the width of the apertures from d to an effective width of $d+2\delta_{\text{InSb}}$ [41]. The temperature depen-
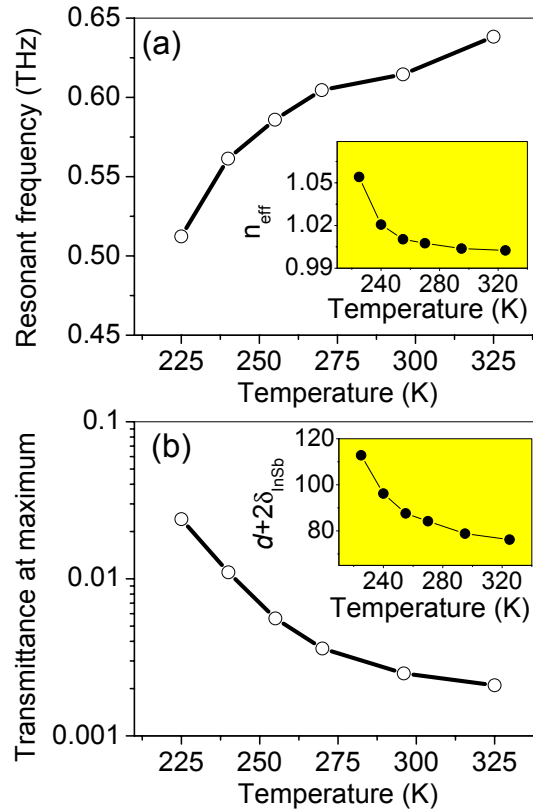
Fig. 7. Temperature dependence of the resonance frequency (a) and of the maximum transmittance at the resonance (b). The inset of (a) represents the effective refractive index as a function of temperature and that of (b) is the effective aperture size.

dence of the effective aperture width is represented in the inset of Fig. 7(b). Since the transmission through subwavelength apertures depends strongly on their size [19], the increase of the effective aperture size modifies it. As the size of the apertures increases, the cutoff frequency shifts to lower values and the subwavelength transmission at a given frequency increases. Also, the fraction of the surface effectively occupied by apertures increases which leads to a larger transmission.

The high fragility of InSb made impossible to structure gratings with apertures wider than 70 μm. Silicon is less brittle and easier to process than InSb. Therefore, to illustrate the influence of the size of the apertures on the transmittance, we have measured the transmission through gratings structured in doped silicon with aperture sizes of 70, 110 and 130 μm. A detailed description of these gratings can be found in Ref. [19], here we should only mention that the gratings were structured as described in section 2.2 and have a thickness of 100 μm, a lattice constant of 400 μm, and the depth of the cuts is 50 μm. The transmittance measurements through these gratings are plotted in Fig. 8. The inset of this figure represents the same measurements plotted on a logarithmic scale. The increase of the transmission with the size of the apertures is apparent. It is remarkable that the resonant frequency does not change appreciably as might be expected since the permittivity of Si is the same in the three samples, and consequently n_{eff} does not change.

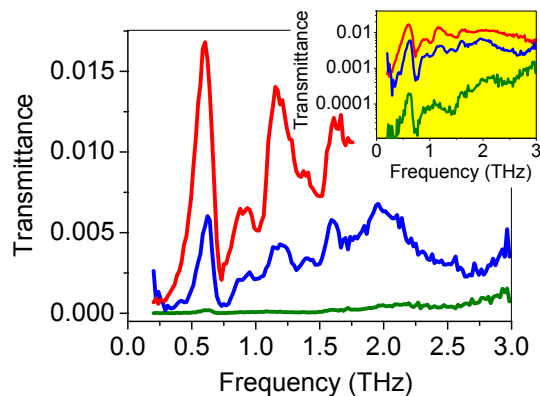A negative effect in the transmission is caused by losses in the apertures. Radiation transmit-

Fig. 8. Transmittance through silicon gratings with lattice constant of 400 μm and different apertures sizes. The red line corresponds to the transmittance through a grating with square apertures with a lateral size of 130 μm, while the blue and green lines are the transmittance through similar gratings with apertures sides of 110 and 70 μm respectively.

ted through a waveguide might be absorbed at the walls if the conductivity is not infinite [42], or in other words, if $\delta_{InSb} > 0$. These losses are more important at low temperatures, where one should expect that the transmission through the subwavelength apertures decreases. This behavior was observed in gratings structured in doped silicon [20]. However, we only observe an increase of the transmission through the InSb gratings as the temperature is reduced, which stems from the fact that at temperatures lower than 225 K the transmission through bulk InSb is dominant and the grating becomes optically thin.

Finally, we should mention that the change of the decay length of SPPs into air δ_{air} with temperature (see Table 1) may play as well a role. At low temperatures SPPs are better confined to the surface, i.e., δ_{air} is smaller, which should favor the transmission [12].

Summarizing, the dependence of the subwavelength transmission with temperature merges as the result of several mechanisms, which have different effects on the transmission. For InSb gratings, the large skin depth at low temperatures leads to an increase of the transmission. This is in contrast with the reduction of the transmission through doped Si gratings at low temperatures reported in Ref. [20], and with the temperature independent transmission through metallic gratings. A quantitative description of the phenomenon is not yet available and further theoretical investigations are necessary.

5. Conclusions

Transmission measurements of THz radiation through gratings of apertures structured in InSb have been presented. In agreement with optical experiments on gratings of nanoholes, we observe significant transmission of frequencies well below the cutoff defined by the apertures. This transmission has been interpreted by the excitation of terahertz SPPs in semiconductors. By varying the temperature of the grating, the permittivity of InSb and the SPPs characteristics change, leading to a variation of the subwavelength transmission. In a temperature range of 100 K the subwavelength transmission shifts more than 100 GHz and increases by more than one order of magnitude. This increase is mainly attributed to a variation of the skin depth of InSb which leads to an effective aperture size larger than the nominal aperture size.

Acknowledgments